DALTON
FULL PAPER

Micro-Raman study of perovskites in the $CaTiO_3$–$SrTiO_3$ system

Shan Qin,[a] Xiang Wu,[a] Friedrich Seifert[b] and Ana I. Becerro*†[b]

[a] *Department of Geology, Peking University, Beijing 100871, China*
[b] *Bayerisches Geoinstitut, Universität Bayreuth, D-95440 Bayreuth, Germany*

Received 15th March 2002, Accepted 25th July 2002
First published as an Advance Article on the web 3rd September 2002

The perovskite compounds $Ca_{1-x}Sr_xTiO_3$ ($0 \le x \le 1$) have been studied by Raman spectrometry at room temperature. Following the intensity of selected bands, we have confirmed the sequence of phase transitions with increasing Sr content from orthorhombic *Pbnm* through tetragonal *I*4/*mcm* to cubic, and the phase boundaries have been located near $x = 0.67$ and $x = 0.95$, respectively. The Raman spectra gave no indication of a *Bmmb* structure. With increasing x, all the Raman modes shift to lower frequency, the shift being more pronounced in the low frequency bands. These frequency shifts have been related to structural information obtained from X-ray diffractometry. Linear relationships are observed between the behaviour of structural parameters, such as the Ca(Sr)–O distance and the octahedral tilt angle, and the corresponding Raman frequency shifts.

Introduction

$CaTiO_3$ and $SrTiO_3$ are typical perovskite materials and their structures in the system $CaTiO_3$–$SrTiO_3$ have been extensively investigated. Due to a ≈17% difference in ionic radius between Sr^{2+} and Ca^{2+}, the local distortions associated with substituting Sr for Ca are expected to impact on the phase transitions of $Ca_{1-x}Sr_xTiO_3$ which can be explained in terms of octahedral tilting,[1,2] *i.e.* the lower symmetry structures of *Pnma* (and/or *Bmmb*) and *I*4/*mcm* for $Ca_{1-x}Sr_xTiO_3$ can be derived from the prototype *Pm*3*m*, $SrTiO_3$. At room temperature, the $CaTiO_3$ end member exhibits the orthorhombic space group *Pbnm*, an unconventional setting for *Pnma*,[3] while the $SrTiO_3$ end member is cubic with space group *Pm*3*m*.[4] The structures and the phase boundaries in the intermediate phases for $Ca_{1-x}Sr_xTiO_3$ ($0 < x < 1$) are still controversial.[5–8] Especially, in the range with $x = 0.4$–0.6, the structure of $Ca_{1-x}Sr_xTiO_3$ has been strongly debated by different researchers. Ball *et al.*[9] reported an orthorhombic *Bmmb* structure for $Ca_{1-x}Sr_xTiO_3$ when $0.45 \le x \le 0.60$ by a study of synchrotron diffraction. However, Ranjan and Pandey[10,11] and Ranjan *et al.*[12] suggested that the structure remains orthorhombic until $x \approx 0.88$, and that no *Bmmb* structure exists in the entire system. Our previous study on the same system by calorimetry and by X-ray diffraction at room temperature[13] drew similar conclusions as Ball *et al.*,[9] but the evidence for the *Bmmb* phase was weak, either due to the limited resolution of our diffractometer or because the *Bmmb* phase may not have a stability field at this composition. More recently, based on the analyses of neutron and electron diffraction, Howard *et al.*[14] argued that the space group of perovskite $Ca_{0.5}Sr_{0.5}TiO_3$ at room temperature is not *Cmcm* (equivalent to *Bmmb*) but *Pnma*, and they concluded that the most likely sequence of structures of $Ca_{1-x}Sr_xTiO_3$ is *Pnma*, *I*4/*mcm* and *Pm*3*m* with the phase boundaries at $x = 0.65$ and $x = 0.92$, respectively. In an infrared spectroscopic study, Meyer *et al.*[15] found no clear evidence for a *Bmmb* structure either and concluded that perovskites in the central portion of the phase diagram exhibit a maximum of disorder.

Raman spectroscopy is a sensitive indicator of structure and symmetry in solids and has proved to be useful in the study of phase transitions as a function of temperature,[16] pressure[17] and composition.[18] The room temperature Raman spectrum of polycrystalline $CaTiO_3$ was first reported by Balachandran and Eror,[19] in which the authors assigned all the bands to first-order Raman scattering and interpreted the spectrum in terms of stretching and bending vibrations and external modes. McMillan and Ross[20] showed a similar unpolarized spectrum of $CaTiO_3$, but they assigned the broad features at 150–600 and 650–850 cm^{-1} to second-order Raman scattering. Gillet *et al.*[21] also took Raman spectra on $CaTiO_3$ at 300 K and 110 K, and new first-order bands at 623 and 640 cm^{-1} and between 340 and 470 cm^{-1} were revealed in the lower temperature spectrum. The other end member, $SrTiO_3$, is cubic at room temperature and shows strong second-order Raman scattering between 200 and 500 cm^{-1}, and 600–800 cm^{-1},[22–24] as well as a sharp band near 80 cm^{-1}.[20] Mishra *et al.*[25] carried out a Raman scattering measurement on $Ca_{0.30}Sr_{0.70}TiO_3$ as a function of temperature; however, the room temperature Raman measurements on intermediate members of the solid solution $Ca_{1-x}Sr_xTiO_3$ were reported, to our knowledge, only once in the literature by Hirata *et al.*[8] The authors only analysed the frequency shift of the band at 460 cm^{-1} and related it to the stronger interaction of the smaller Ca^{2+} with the oxygens, which produces a distortion of the octahedron.

As a technique sensitive to structural distortions and short-range order, Raman spectroscopy is taken here to re-examine the phase transitions and structural distortions in the $Ca_{1-x}Sr_xTiO_3$ system. We present a systematic study of the Raman active phonon modes of various possible crystallographic phases in this solid solution. A comparison of the experimental data with a group theoretical analysis of the allowed zero-wave-vector ($q \approx 0$) phonon modes for the respective structures has been made to identify the presence of different symmetry phases and to estimate transition compositions. Finally, structural distortion parameters have been calculated by means of X-ray diffraction and their relationship with the Raman scattering has been characterized.

Experimental

15 powder samples, the same as used in our previous study, in the $Ca_{1-x}Sr_xTiO_3$ system with nominal compositions $x = 0$ to 1 were employed. Details for sample synthesis can be found in

† Present address: Departamento de Química Inorganíca–Instituto de Ciencia de Materiales, Universidad de Sevilla-CSIC, Avda. Américo Vespucio s/n, 41092 Sevilla, Spain. E-mail: anieto@icmse.csic.es

ref. 13. The microprobe analysis showed the materials to be close to the nominal composition and homogeneous at the 1% level.

The Raman spectra for $Ca_{1-x}Sr_xTiO_3$ powder samples were measured, in the range of 100–750 cm^{-1}, using a laser Raman spectrometer (LabRam-010, France). The 632.817 nm He–Ne laser was taken as an exciting source with 15 mW power. A Leica optical microscope with an 40× objective was used to focus the emission line, and a 10× objective to collect the back-scattered radiation. The scattering light dispersed by the spectrophotometer was detected by a charge-coupled device (CCD) detecting system, with an 1800 grooves per mm^2 grating Spectral resolution was typically around 1 cm^{-1}. All the Raman spectra were recorded at room temperature in a backscattering geometry.

X-Ray diffraction patterns at room temperature were measured on a Siemens D-5000 diffractometer with Cu-K$\alpha_{1,2}$ radiation and were reported in our previous study.[13] We have now taken the atomic position values, calculated by Rietveld refinement, to obtain Ca(Sr)–O distances and out-of-phase tilt angles. The out-of-phase tilt angles are estimated from the atomic displacements of the O2 oxygen atoms from (¼, ¼, 0) to (¼ − u, ¼ + v, w) and tan $\varphi = 4\sqrt{2}w$ for the *Pbnm* phase (x = 0–0.6), and tan $\varphi = 4u$ for the *I*4/*mcm* phase (x = 0.7–0.9). For details, see Kennedy *et al.*[26]

Symmetry of phases and Raman selection rules

As mentioned above, the most likely sequence of phases in the $Ca_{1-x}Sr_xTiO_3$ system, with increasing x at room temperature, is from *Pbnm* to *Bmmb* to *I*4/*mcm* to *Pm*3*m*. The Raman active phonon modes of various possible crystallographic phases have been predicted by factor group analysis, and the results are presented in Table 1(a–d) corresponding to *Pbnm*, *Bmmb*, *I*4/*mcm* and *Pm*3*m* structures, respectively. For the orthorhombic *Pbnm*, it yields 24 Raman active phonon modes of irreducible representations $7A_g + 5B_{1g} + 7B_{2g} + 5B_{3g}$ (see also Iliev *et al.*,[27] and Genet *et al.*[28]). Comparing Table 1(a) with 1(b), one can find that *Pbnm* and *Bmmb* have the same kinds of Raman active phonons (A_g, B_{1g}, B_{2g}, B_{3g}), but the number of Raman active modes for *Bmmb* is double that of *Pbnm*. Therefore a transition from *Pbnm* to *Bmmb* will induce splitting of peaks in the Raman spectrum. On the other hand, the tetragonal *I*4/*mcm* phase has only 14 Raman active phonons $2A_g + 4B_{1g} + 2B_{2g} + 6E_g$ [Table 1(c)]. The decrease in the number of phonon modes from 24 (or 48 for *Bmmb*) to 14 on going from the ortho-rhombic to the tetragonal structure is due to an increase in symmetry, merging nondegenerate $B_{2g} + B_{3g}$ phonons into degenerate E_g phonons and annihilating some A_g. For cubic *Pm*3*m* [Table 1(d)], there is only one formula unit per unit cell and apart from an infrared active F_{1u} phonon, no first-order Raman bands are expected. The first-order Raman scattering of A_{1g} and E_g modes turn into the Raman inactive F_{1u} soft mode; the $E_g + B_{1g}$ mode transforms to the so-called silent mode F_{2u} upon the transition from tetragonal to cubic.[29] In other words, all first-order Raman bands will disappear on the transition from orthorhombic or tetragonal to cubic.

On the other hand, the phase transitions observed, from orthorhombic through tetragonal to cubic, may be discussed in terms of mode softening and dynamic instabilities at the Brillouin zone boundary of the ideal cubic perovskite.[20,30,31] Thus, these transitions or distortions occur *via* cooperative rotations of the TiO_6 octahedra at the R and M points of the cubic Brillouin zone with a variation of unit cell size as a function of the Sr concentration.

Results and discussion

Fig. 1 displays the unpolarized Raman spectra of $Ca_{1-x}Sr_xTiO_3$ ($0 \le x \le 1$) in the frequency range 100–750 cm^{-1}. The cubic

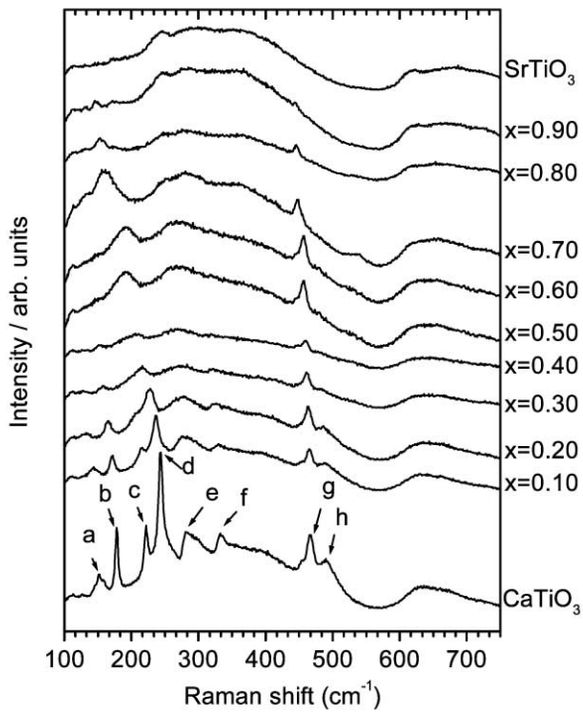

Fig. 1 Unpolarized Raman spectra of pervoskites $Ca_{1-x}Sr_xTiO_3$ ($0 \le x \le 1$) at room temperature. The peaks have been labeled with letters from a to h for easy identification when analysed in the Figures and in Table 2.

phase of $SrTiO_3$ corresponds to space group *Pm*3*m* which has no Raman active modes. Its spectrum is dominated by two strong and broad second-order Raman bands at 200–500 cm^{-1} and 600–750 cm^{-1} in agreement with the literature.[8,20] The Raman spectrum of the other end member, $CaTiO_3$, shows a number of sharp peaks superimposed on a broad feature between 150 and 550 cm^{-1}, and a second broad band between 600 and 750 cm^{-1}. This is in accordance with the spectra obtained by McMillan and Ross[20] and Gillet *et al.*,[21] also similar to the band positions reported by Balachandran and Eror[19] and Hirata *et al.*[8] (except for the higher frequency modes at 639 and 677 cm^{-1} in their spectra). The observed frequencies of Raman modes and their assignments compared with those reported for $CaTiO_3$ in the literature are given in Table 2. As seen in Fig. 1 and Table 2, fewer bands are observed in the Raman spectra than were predicted by the factor group analysis, possibly due to peak overlap or very low polarizabilities so as to prevent such bands from being seen in the spectrum.

With increasing Sr content, all the bands observed shift toward lower frequency, broaden and weaken in intensity, in good agreement with the observations of Hirata *et al.*.[8] The lower frequency Raman modes have larger frequency shifts than those in the higher frequency range (Fig. 2). For instance, the band at 244 cm^{-1} shifts to 141 cm^{-1} with increasing Sr content from x = 0 to x = 0.9, while the band at 467 cm^{-1} decreases only to 444 cm^{-1} in the same x range. The band of A_g symmetry at 178 cm^{-1}, associated with the O–Ti–O bending mode, might be diagnostic for the transition from ortho-rhombic to tetragonal.[32] When we draw the intensities of this band as a function of $SrTiO_3$ content (Fig. 3 left), the extra-polation shows that the boundary from orthorhombic to tetra-gonal is near $x \approx 0.67$. The band at 467 cm^{-1}, which would be correlated with the A_g mode and described as a TiO_6 distorted octahedron with large Ti–O stretching,[19,20] could be diagnostic of the phase transition from *I*4/*mcm* to *Pm*3*m*.[33] Similarly, when the intensities for the 467 cm^{-1} band are plotted *versus* Sr content (Fig. 3 right), the extrapolation gives the phase transition at $x \approx 0.95$. The phase boundaries located by Raman

Table 1 Factor group analysis and selection rules for the zone-center vibrational modes

Atom	Number of equivalent positions (Wyckoff notation)	Site symmetry	Irreducible representations of modes
a. orthorhombic *Pbnm*, $Z = 4$			
Ca(Sr)	4 (c)	C_s	$2A_g + B_{1g} + 2B_{2g} + B_{3g} + A_u + 2B_{1u} + B_{2u} + 2B_{3u}$
Ti	4 (a)	C_i	$3A_u + 3B_{1u} + 3B_{2u} + 3B_{3u}$
O1	4 (c)	C_s	$2A_g + B_{1g} + 2B_{2g} + B_{3g} + A_u + 2B_{1u} + B_{2u} + 2B_{3u}$
O2	8 (d)	C_1	$3A_g + 3B_{1g} + 3B_{2g} + 3B_{3g} + 3A_u + 3B_{1u} + 3B_{2u} + 3B_{3u}$
$\Gamma_{Raman} = 7A_g + 5B_{1g} + 7B_{2g} + 5B_{3g}$		Raman selection rules:	
$\Gamma_{IR} = 9B_{1u} + 7B_{2u} + 9B_{3u}$		A_g: σ_{xx}, σ_{yy} and σ_{zz}	
$\Gamma_{acoustic} = B_{1u} + B_{2u} + B_{3u}$		B_{1g}: σ_{xy}	
$\Gamma_{silent} = 8A_u$		B_{2g}: σ_{xz}	
		B_{3g}: σ_{yz}	
b. orthorhombic *Bmmb*, $Z = 8$			
Ca(Sr)	4 (c)	C_{2v}	$2A_g + 2B_{1g} + 2B_{3g} + 2B_{1u} + 2B_{2u} + 2B_{3u}$
1	4 (c)	C_{2v}	$2A_g + 2B_{1g} + 2B_{3g} + 2B_{1u} + 2B_{2u} + 2B_{3u}$
Ca(Sr)	8 (d)	C_i	$6A_u + 6B_{1u} + 6B_{2u} + 6B_{3u}$
2	8 (e)	C_2	$2A_g + 4B_{1g} + 4B_{2g} + 2B_{3g} + 2A_u + 4B_{1u} + 4B_{2u} + 2B_{3u}$
Ti	8 (f)	C_s	$4A_g + 2B_{1g} + 2B_{2g} + 4B_{3g} + 2A_u + 4B_{1u} + 4B_{2u} + 2B_{3u}$
O1	8 (g)	C_s	$4A_g + 4B_{1g} + 2B_{2g} + 2B_{3g} + 2A_u + 2B_{1u} + 4B_{2u} + 4B_{3u}$
O2			
O3			
$\Gamma_{Raman} = 14A_g + 14B_{1g} + 8B_{2g} + 12B_{3g}$		Raman selection rules:	
$\Gamma_{IR} = 19B_{1u} + 21B_{2u} + 17B_{3u}$		A_g: σ_{xx}, σ_{yy} and σ_{zz}	
$\Gamma_{acoustic} = B_{1u} + B_{2u} + B_{3u}$		B_{1g}: σ_{xy}	
$\Gamma_{silent} = 12A_u$		B_{2g}: σ_{xz}	
		B_{3g}: σ_{yz}	
c. tetragonal *I*4/*mcm*, $Z = 4$			
Ca(Sr)	4 (b)	D_{2d}	$2B_{1g} + 2E_g + 2A_{2u} + 2E_u$
Ti	4 (c)	C_{4h}	$2A_{1u} + 2A_{2u} + 4E_u$
O1	4 (a)	D_4	$2A_{2g} + 2E_g + 2A_{2u} + 2E_u$
O2	8 (h)	C_{2v}	$2A_{1g} + 2A_{2g} + 2B_{1g} + 2B_{2g} + 2E_g + 2A_{2u} + 2B_{1u} + 4E_u$
$\Gamma_{Raman} = 2A_{1g} + 4B_{1g} + 2B_{2g} + 6E_g$		Raman selection rules:	
$\Gamma_{IR} = 7A_{2u} + 11E_u$		A_g: σ_{xx}, σ_{yy} and σ_{zz}	
$\Gamma_{acoustic} + A_{2u} + E_u$		B_{1g}: $\sigma_{x^2-y^2}$	
$\Gamma_{silent} = 4A_{2g} + 2A_{1u} + 2B_{1u}$		B_{2g}: σ_{xy}	
		E_g: σ_{xz} and σ_{yz}	
d. cubic *Pm*3*m*, $Z = 1$			
Sr	1 (b)	O_h	F_{1u}
Ti	1 (a)	O_h	F_{1u}
O	3 (d)	D_{4h}	$2F_{1u} + 2F_{2u}$
$\Gamma_{Raman} = 0$		Raman selection rules: none	
$\Gamma_{IR} = 3F_{1u}$			
$\Gamma_{accoustic} = F_{1u}$			
$\Gamma_{silent} = F_{2u}$			

Table 2 Frequencies (cm^{-1}) of unpolarized Raman bands and their assignments for $CaTiO_3$ perovskite

Bands assignment	Ref. 19	Ref. 20	Ref. 21	Ref. 8	This work	Labels corresponding to Fig. 1
Ca–TiO_3 lattice mode	155	154	155		153	a
O–Ti–O bending modes	180	181	181	175	178	b
	226	225	226	224	222	c
	247	246	248	244	244	d
	286	284	290	286	281	e
		300	302			
	337	337	340	336	333	f
Torsional modes	471	469	470	471	467	g
	495	493	496	492	490	h

scattering are in good agreement with the XRD results of Qin *et al.*[13]

We return to the question of whether an orthorhombic *Bmmb* phase exists in the $CaTiO_3$–$SrTiO_3$ system. Theoretically, for the *Bmmb* structure 48 Raman active modes can be expected (Table 1b). However, in the Raman spectra for the corresponding compositions (Fig. 1), we do not observe any new or split peaks that might be assigned to *Bmmb* rather than *Pbnm*. It is possible that a transition from *Pbnm* to *Bmmb* could not be discerned by Raman scattering, or that there is no *Bmmb* phase as claimed by Howard *et al.*[14] and Ranjan *et al.*[12] This result is therefore similar to that of the other vibrational spectroscopic study (infrared[15]). In addition, we also observe that the orthorhombic Raman active modes of A_g symmetry at 153, 222 and 490 cm^{-1} are broadened with increasing x and disappear simultaneously when $x = 0.40$ (Fig. 1). This could possibly be related to the fact that the perovskite structure is metrically strongly pseudocubic in the range x *ca.* 0.40 to 0.65.[9,13]

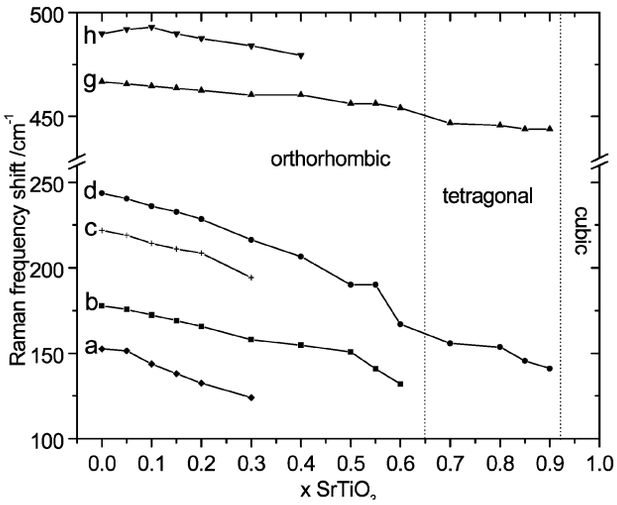

Fig. 2 Observed line positions of selected phonon modes in $Ca_{1-x}Sr_xTiO_3$ ($0 \leq x \leq 1$) as a function of the Sr content x at room temperature. The bands at 281 and 333 cm^{-1} are not plotted in the figure due to the difficulty of locating the peak positions precisely. The phase boundaries marked in the figure have been located by XRD analysis.[13]

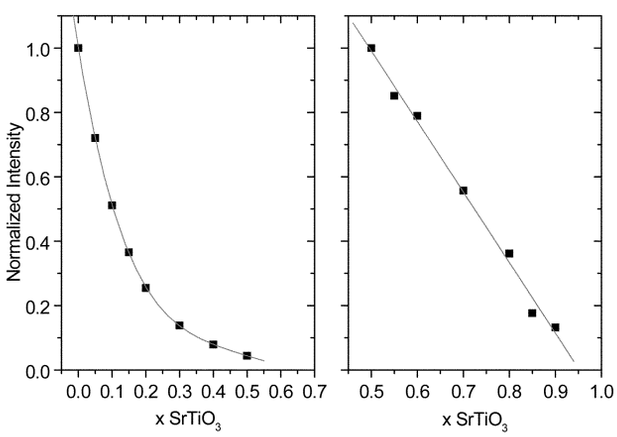

Fig. 3 Variation of the intensity of the Raman bands b (left) and g (right) as a function of Sr content at room temperature in the $Ca_{1-x}Sr_xTiO_3$ system. The regression lines, exponential in the left plot and linear in the right one, serve as a guide to eye only.

The transitions of $Ca_{1-x}Sr_xTiO_3$ from *Pbnm* ($a^+b^-b^-$), through *Bmmb* ($a^0b^+c^-$) or *I*4/*mcm* ($a^0a^0c^-$), to *Pm*3*m* ($a^0a^0a^0$) involve the disappearance of octahedral rotations. Thus, the metal–oxygen bond distances and tilt angles are expected to change systematically with composition. Fig. 4 shows the behaviour of both the out-of-phase tilt angle and the Ca(Sr)–O distance with increasing Sr content, as calculated from X-ray diffraction. The out-of-phase tilt angle decreases in a clearly non-linear manner when going from the orthorhombic to the tetragonal and cubic fields. A similar behaviour was reported by Kennedy *et al.*[26] for the $CaTiO_3$ end-member with increasing temperature. $CaTiO_3$ transforms from orthorhombic to tetragonal and cubic symmetry on going from room temperature to high temperatures, and it is, therefore, reasonable that the behaviour of the out-of-phase angle is similar in both cases. On the other hand, Fig. 4 shows the linear increase of the Ca(Sr)–O distance with increasing Sr content, as expected from the higher ionic radius of Sr^{2+} as compared with Ca^{2+}.

Raman spectroscopy, as a technique sensitive to short-range order, must give information of small structural distortions, and the Raman frequency shifts are, therefore, expected to contain information about structural parameters such as Ca(Sr)–O distance and octahedral tilt angle. The frequency shift of the band corresponding to the Ca–TiO_3 lattice mode (labeled a in Fig. 1 and Table 2) must be directly related to the Ca(Sr)–O distance; we have plotted both parameters in Fig. 5, and a

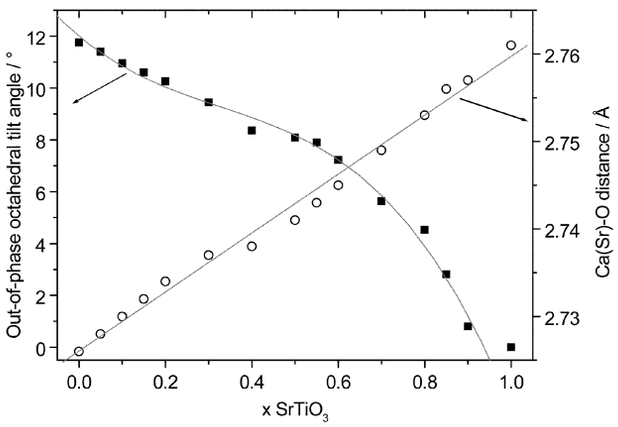

Fig. 4 Octahedral out-of-phase tilt angle (■) and Ca(Sr)–O distance (○) *versus* Sr content for $Ca_{1-x}Sr_xTiO_3$ perovskites. The lines are guides to the eye.

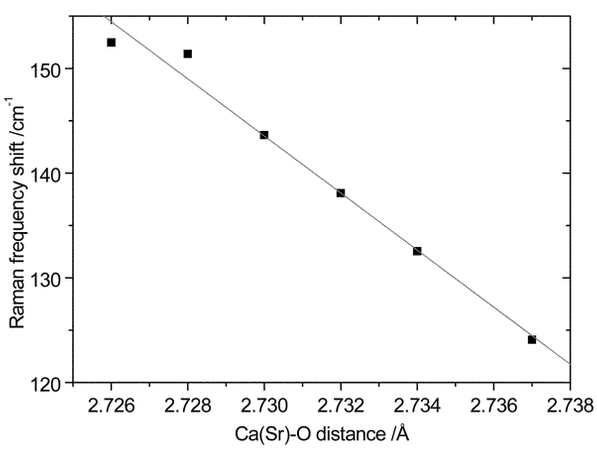

Fig. 5 Raman frequency shift dependence of the Ca–TiO_3 lattice mode (labeled a in Table 2) on the average Ca(Sr)–O distance for $Ca_{1-x}Sr_xTiO_3$ perovskites.

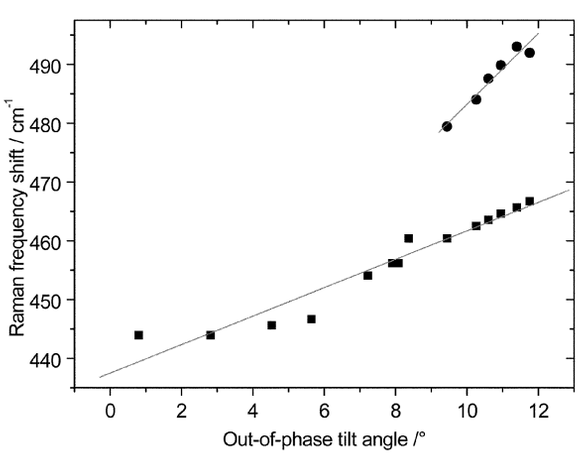

Fig. 6 Raman frequency shift dependence of the the torsional modes g (■) and h (●) on the out-of-phase octahedral tilt angle for $Ca_{1-x}Sr_xTiO_3$ perovskites.

clearly linear relationship is observed between them. On the other hand, the two torsional modes (bands g and h in Fig. 1 and Table 2) are expected to be dependent on the tilt angle of the octahedra. Fig. 6 is a representation of the Raman frequency shift of both bands *versus* the out-of-phase tilt angle for each composition. Again a quasi-linear relationship is observed, although, in this case, other factors must also affect the frequency shifts as inferred from the different slopes of both lines as well as from the slight deviation of the data points from the linear regression curves.

Conclusions

Powder samples of the perovskite $Ca_{1-x}Sr_xTiO_3$ ($0 \leq x \leq 1$) have been characterized by Raman spectroscopy. Comparing the experimental Raman data with the theoretical analysis, we confirm that the sequence of phase transitions is orthorhombic *Pbnm*, tetragonal *I*4/*mcm* and cubic *Pm*3*m* with increasing Sr content, and the phase boundaries at room temperature are located near $x \approx 0.67$ and ≈ 0.95 for *Pbnm* to *I*4/*mcm* and *I*4/*mcm* to *Pm*3*m*, respectively. These values are very close to the boundaries obtained in our previous room temperature XRD analyses on the same samples. The Raman data give no indication of a *Bmmb* structure. Linear relationships are observed between the behaviour of structural parameters, indicative of the short range order of the structure, and the corresponding Raman frequency shifts.

Acknowledgements

The authors thank Professor Zhou Yaoqi and his Raman Laboratory at the University of Petroleum, China for their support in carrying out the Raman measurements. This work was partly supported by the National Key Program for Basic Research (No. 2001CCA02400) from the Ministry of Science and Technology, China.

References

1 A. M. Glazer, *Acta Crystallogr., Sect. B*, 1972, **28**, 3384–3392.
2 P. M. Woodward, *Acta Crystallogr., Sect. B*, 1997, **53**, 44–66.
3 S. Sasaki, T. Prewitt, J. D. Bass and W. A. Schulze, *Acta Crystallogr., Sect. C*, 1987, **43**, 1668–1674.
4 R. H. Buttner and E. N. Maslen, *Acta Crystallogr., Sect. B*, 1992, **48**, 639–649.
5 M. McQuarrie, *J. Am. Ceram. Soc.*, 1955, **38**, 444–449.
6 T. Mitsui and W. B. Westphal, *Phys. Rev.*, 1961, **124**, 1354–1359.
7 M. Ceh, D. Kolar and L. Golic, *J. Solid State Chem.*, 1987, **68**, 68–72.
8 T. Hirata, K. Ishioka and M. Kitajima, *J. Solid State Chem.*, 1996, **124**, 353–359.
9 C. J. Ball, B. D. Begg, D. J. Cookson, G. J. Thorogood and E. R. Vance, *J. Solid State Chem.*, 1998, **139**, 238–247.
10 R. Ranjan and D. Pandey, *J. Phys.: Condens. Matter*, 1999, **11**, 2247–2258.
11 R. Ranjan and D. Pandey, *J. Phys.: Condens. Matter*, 2001, **13**, 4251–4266.
12 R. Ranjan, D. Pandey, W. Schuddinck, O. Richard, P. D. Meulenaere, J. Van Landuyt and G. Van Tendeloo, *J. Solid State Chem.*, 2001, **162**, 20–28.
13 S. Qin, A. I. Becerro, F. Seifert, J. Gottsmann and J. Jiang, *J. Mater. Chem.*, 2000, **10**, 1609–1615.
14 C. J. Howard, R. L. Withers and B. J. Kennedy, *J. Solid State Chem.*, 2001, **160**, 8–12.
15 H. W. Meyer, M. A. Carpenter, A. I. Becerro and F. Seifert, *Am. Mineral.*, 2002, in press.
16 A. N. Vtyurin, A. Bulou, A. S. Krylov, M. L. Afanasev and A. Shebanin, *Phys. Solid State*, 2001, **43**, 2307–2310.
17 T. Sekiya, S. Ohta, S. Kamei, M. Hanakawa and S. Kurita, *J. Phys. Chem. Solids*, 2001, **62**, 717–721.
18 P. S. Dobal, A. Dixit, R. S. Katiyar, D. García, R. Guo and A. S. Bhalla, *J. Raman Spectrosc.*, 2001, **32**, 147–149.
19 U. Balachandran and N. G. Eror, *Solid State Commun.*, 1982, **44**, 815–818.
20 P. McMillan and N. Ross, *Phys. Chem. Miner.*, 1988, **16**, 21–28.
21 P. Gillet, F. Guyot, G. D. Price, B. Tournerie and A. L. Cleach, *Phys. Chem. Miner.*, 1993, **20**, 159–170.
22 C. H. Perry, J. H. Fertel and T. F. McNelly, *J. Chem. Phys.*, 1967, **47**, 1619–1625.
23 W. G. Nilsen and J. G. Skinner, *J. Chem. Phys.*, 1968, **48**, 2240–2248.
24 W. G. Stirling, *J. Phys. C: Solid State Phys.*, 1972, **5**, 2711–2730.
25 S. K. Mishra, R. Ranjan, D. Pandey, R. Ouillon, J. P. Pinan-Lucarre, P. Ranson and P. Pruzan, *Phys. Rev. B*, 2001, **64**, 2302–2305.
26 B. J. Kennedy, C. J. Howard and B. C. Chakoumakos, *J. Phys.: Condens. Matter*, 1999, **11**, 1479–1488.
27 M. N. Iliev, M. V. Abrashev, H. G. Lee, V. N. Popov, Y. Y. Sun, C. Thomsen, R. L. Meng and C. W. Chu, *Phys. Rev. B*, 1998, **57**, 2872–2877.
28 F. Genet, S. Loridant, C. Ritter and G. Lucazeau, *J. Phys. Chem. Solids*, 1999, **60**, 2009–2021.
29 P. S. Dobal, A. Dixit, R. S. Katiyar, D. Garcia, R. Guo and A. S. Bhalla, *J. Raman Spectrosc.*, 2001, **32**, 147–149.
30 P. A. Fleury, J. F. Scott and J. M. Worlock, *Phys. Rev. Lett.*, 1968, **21**, 16–19.
31 D. J. Durben, G. H. Wolf and P. F. McMillan, *Phys. Chem. Miner.*, 1991, **18**, 215–223.
32 E. Cockayne and B. P. Burton, *Phys Rev. B*, 2000, **62**, 3735–3743.
33 U. Bianchi, W. Kleemann and J. G. Bednorz, *J. Phys.: Condens. Matter*, 1994, **6**, 1229–1238.